Molecular Medicine

Development of a Zebrafish Sepsis Model for High-Throughput Drug Discovery

Anju M Philip,[1,2,3] Youdong Wang,[1,2] Antonio Mauro,[1,2,4,6] Suzan El-Rass,[1,2,4,6] John C Marshall,[1,2,5] Warren L Lee,[1,2,4] Arthur S Slutsky,[1,2,4,5] Claudia C dos Santos,[1,2,4,5] and Xiao-Yan Wen[1,2,3,4,6]

[1]Zebrafish Centre for Advanced Drug Discovery, St. Michael's Hospital, Toronto, Ontario, Canada, [2]Keenan Research Centre for Biomedical Science and Li Ka Shing Knowledge Institute of St. Michael's Hospital, Toronto, Ontario, Canada, [3]Department of Physiology, [4]Department of Medicine and Institute of Medical Science, [5]Interdepartmental Division of Critical Care, and [6]Collaborative Program in Cardiovascular Sciences, Faculty of Medicine, University of Toronto, Toronto, Ontario, Canada

Sepsis is a leading cause of death worldwide. Current treatment modalities remain largely supportive. Intervention strategies focused on inhibiting specific mediators of the inflammatory host response have been largely unsuccessful, a consequence of an inadequate understanding of the complexity and heterogeneity of the innate immune response. Moreover, the conventional drug-development pipeline is time-consuming and expensive, and the low success rates associated with cell-based screens underline the need for whole-organism screening strategies, especially for complex pathological processes. Here, we established a lipopolysaccharide (LPS)-induced zebrafish endotoxemia model, which exhibits the major hallmarks of human sepsis, including edema and tissue/organ damage, increased vascular permeability and vascular leakage accompanied by altered expression of cellular junction proteins, increased cytokine expression, immune cell activation and reactive oxygen species (ROS) production, reduced circulation and increased platelet aggregation. We tested the suitability of the model for phenotype-based drug screening using three primary readouts: mortality, vascular leakage and ROS production. Preliminary screening identified fasudil, a drug known to protect against vascular leakage in murine models, as a lead hit, thereby validating the utility of our model for sepsis drug screens. This zebrafish sepsis model has the potential to rapidly analyze sepsis-associated pathologies and cellular processes in the whole organism, as well as to screen and validate many compounds that can modify sepsis pathology *in vivo*.
Online address: http://www.molmed.org
doi: 10.2119/molmed.2016.00188

INTRODUCTION

Sepsis is defined as life-threatening organ dysfunction caused by a dysregulated host response to infection (1). The systemic response to infection is biologically complex, redundant, activated by both infectious and noninfectious triggers, and poorly understood in humans. In addition, much of immunobiology cannot be examined physiologically in humans because of the inaccessibility of certain tissues or cell types. Reliance on *a priori* biological knowledge and availability of interventions to alter outcomes in preclinical models have failed in translation to the clinic (2).

While studies of cultured cells have led to new insights, greater understanding of putative candidates requires the development of experimental systems that permit analysis of intercellular communication and tissue-tissue interactions in a more relevant organ context. Although alternatives such as the "organ on a chip" offer unique opportunities to study interactions between different cell types (3), these still fall short relevant to whole animals, where the impact of innate immune dysfunction can be studied at an organismal level.

Traditional approaches to target discovery are slow and often take years (4). The list of possible targets is enormous, and the chance is small that targeting any one of these will result in a dramatic improvement in survival. Accordingly, there is a need for better approaches to expedite the pipeline for drug discovery. Phenotype-based screening in whole organisms allows for testing of novel compounds while evaluating complex biological processes at the whole-organism level in an unsupervised and systematic fashion, enhancing the potential to detect more plausible targets for

Address correspondence to *Xiao-Yan Wen, Zebrafish Centre for Advanced Drug Discovery, St. Michael's Hospital, 209 Victoria Street, LKSKI, Room 519, Toronto, ON, M5B 1T8, CA. Phone: 416-847-1737; Fax: 416-864-5476; E-mail: X.Wen@utoronto.ca. CC dos Santos, Interdepartmental Division of Critical Care, St. Michael's Hospital/University of Toronto, 30 Bond Street, Room 4-008, Toronto, ON, M5B 1WB, CA. Phone: 416-864-6060 x 3198; E-mail: DosSantosC@smh.ca.*
Submitted August 30, 2016; Accepted for Publication May 23, 2017; Published Online June 7, 2017 (www.molmed.org)

Feinstein Institute for Medical Research
Northwell Health™

both preclinical and mechanistic studies. While the mouse remains indispensable to preclinical studies, several aspects of murine biology, such as cost, time and drug quantities needed during the drug discovery and development phases, limit its routine use in large-scale genetic and therapeutic screening for drug discovery.

The zebrafish has recently emerged as a powerful vertebrate model to study human pathologies (5). With a sequenced genome, the zebrafish offers a unique and robust prototype for disease modeling because of: (1) its remarkable physiological similarity and degree of functional conservation in basic cell-biological processes to humans, (2) the relative ease of embryonic manipulation and whole-body imaging, (3) high fecundity, (4) low cost and (5) transparency, and (6) the availability of various molecular tools for forward-reverse genetics and genome editing (5). Comparisons between the zebrafish and human reference genomes show that approximately 70% of human genes have at least one obvious zebrafish orthologue (6). In drug research, zebrafish embryos are ideal for high-throughput *in vivo* drug screening and amenable to automation. The zebrafish combines the biological complexity of *in vivo* models with the ease of high-throughput screening and quick assessment of potential toxicity and off-target effects (7). It is expected that the lead compounds identified from this *in vivo* screen targeting entire disease pathways will have a higher success rate than cell-based *in vitro* screens (8).

In the last decade, the zebrafish has been adopted in various fields of immunology as an excellent model to study infectious diseases, inflammatory disorders, cancers and other immune-related diseases (9,10). Zebrafish share the same major blood lineages found in mammals (11). Their innate immune system becomes active during somitogenesis, with fully functional macrophages and neutrophils appearing by 16 hours post-fertilization (HPF) and 26 HPF, respectively (12). Moreover, the transcriptional signatures of their innate immune response resemble those seen in mammals and cell culture systems (9). The zebrafish adaptive immune response does not become active until after approximately three weeks of development, meaning that it can be studied in isolation during the early larval stages, in the absence of T- and B-cell responses (9). Moreover, the fact that the major pathogen recognition receptors (PRRs) and their downstream signaling pathways and innate effector mechanisms are conserved between humans and zebrafish makes the zebrafish an excellent model to study diseases of the innate immune system (9,13). However, there has been some controversy regarding the mechanism of endotoxin recognition in fish. Though lipopolysaccharide (LPS) is a well-established immunostimulant in fish studies, It has been reported that, unlike in humans, recognition of LPS in fish does not occur via TLR4 (14,15). In fact, most fish species (zebrafish is an exception) lack a TLR4, and therefore the molecular mechanisms involved in LPS signaling in teleost models are less clear (16). Yet, activation of downstream signaling molecules like NFκB and MyD88 and the resultant release of proinflammatory cytokines appears to be a conserved response between teleosts and mammals.

Sepsis encompasses a full range of responses, from systemic inflammatory response to organ dysfunction to multiorgan system failure and ultimately death. Patients exhibit an overwhelming inflammatory response to infection in the initial phases of the disease. This is largely due to the activation of immune cells and release of proinflammatory cytokines (IL-1, IL-6, tumor necrosis factor (TNF) and IL-8) during this stage. This systemic inflammatory cascade is initiated by various bacterial products, such as endotoxin (16). These in turn bring about numerous changes at the microvascular and cellular levels, including diffuse activation of inflammatory and coagulation cascades, vasodilation, capillary endothelial leakage, vascular maldistribution and the resulting dysfunctional utilization of oxygen and nutrients at the cellular level. The end results are microvascular thrombosis and microvascular plugging, hypoperfusion, ischemia and tissue injury, which progresses to multiorgan system failure and finally death. Though the body does try to regulate the initial hyperinflammatory state by producing antiinflammatory mediators (IL-10), clinically observed as a period of immunodepression, persistence of this hyporesponsive state is associated with an increased risk of secondary infections and death (17,18).

Endotoxin recapitulates many of the critical findings characteristic of sepsis, including loss of vascular integrity, generation of exudative edema, neutrophil extravasation, immune cell activation with increased proinflammatory and reactive oxygen species (ROS) synthesis, and microcirculatory and coagulation dysfunction. Here, we present and validate a novel zebrafish model of endotoxemia, which we hope can accelerate sepsis drug discovery for phenotype-based chemical screens to identify novel therapeutic targets and compounds with disease-modifying potential.

MATERIALS AND METHODS

Zebrafish Strains and Care

Adult and embryonic zebrafish were raised and maintained using standard laboratory procedures (19–21). Zebrafish were raised on a 14 h/10 h light/dark cycle at 28.5 ± 0.5°C. Embryos were obtained via natural mating and cultured in embryo media. All experiments in this study were carried out according to the ethical guidelines established by the St. Michael's Hospital Animal Committee with approved animal protocol ACC660. Embryos older than 24 HPF were treated with 200 μM 1-phenyl-2-thiourea to block pigmentation.

LPS-Induced Zebrafish Sepsis Model: Survival Curve and Phenotype Analysis

The commonly used murine sepsis models are the LPS and cecal ligation and puncture models (22). In view of practicality, LPS was used in this study to generate a zebrafish sepsis model. Survival analysis for zebrafish exposed to various

concentrations of LPS (*Escherichia coli* 0111:B4; Sigma) was performed. Larvae at 3 d post-fertilization (DPF) were exposed to LPS by immersion technique. Larvae were treated with 25, 50, 75, 100 and 200 μg/mL LPS (dissolved in embryo media) by static immersion at 28.5°C for 2, 7, 9 and 24 h in a total volume of 2 mL per treatment. Control larvae were exposed to embryo media. Treatment was conducted using triplicate groups of 10 larvae per treatment. Phenotypes were also analyzed in 40 larvae/LPS concentration at 6 h post LPS exposure.

Measuring LPS-Induced Vascular Leakage

Microangiography contrast agents quantum dots (QD605) (23) and fluorescein isothiocyanate (FITC)-dextran (4 KD) were used to visualize loss of endothelial barrier function and vascular leakage.

Three DPF *Tg (flk1*: GFP) and *Tg (kdrl*: mcherry) larvae were exposed to LPS (100 μg/mL) by static immersion for 6 h at 28.5°C. Control larvae were exposed to embryo media. The larvae were then anesthetized in clove oil and QD605 (an average of 3 trials of 9–14 larvae per treatment) or FITC dextran (4KD; an average of 3 trials of 10–15 larvae per treatment) was injected into the common cardinal vein (CCV) of the *Tg (flk1*: GFP) or *Tg (kdrl*: mcherry) larvae, respectively, using standard microinjection protocols. The injected embryos were transferred to embryo media and allowed to recover, then imaged 30 min after injection using a Leica fluorescence microscope (Leica Microsystems, Wetzlar, Germany). For real-time visualization of vascular leakage, immediately after recovery from FITC-dextran injection, control and LPS-treated larvae were immobilized in low-melting-point agarose and subjected to time-lapse imaging using the Leica fluorescence microscope.

Measuring Expression of Cytokines and Cellular Junction Proteins

Semiquantitative reverse transcription polymerase chain reaction (RT-PCR) was used to assess relative expression of cytokines (an average of 3 trials, each trial with a pool of 20 larvae/treatment) and cellular junction proteins (an average of 3–5 trials, each trial with a pool of 20 larvae/treatment), using *elongation factor 1 α* (*EF1α*) as the housekeeping gene control.

RNA extraction and cDNA synthesis. Three DPF wild-type zebrafish larvae were exposed to LPS (100 μg/mL) by static immersion for 6 h at 28.5°C. Control larvae were exposed to embryo media. Total RNA was extracted from these larvae (pool of 20 larvae/treatment) using the RNeasy extraction kit (Qiagen, Mississauga, Ontario, Canada) and treated with DNase. The concentration of total RNA was determined spectrophotometrically at 260/280 nm using a NanoDrop™ spectrophotometer. First-strand cDNA was synthesized from 1μg of total RNA using the Superscript II reverse transcriptase kit (Invitrogen) according to the manufacturer's instructions.

PCR conditions. The genes of interest and the primer pairs used are given in Table 1. Amplification of cDNA was achieved with an initial denaturation at 94°C for 2 min followed by 40 cycles of denaturation (94°C for 30 s), annealing (58°C for 30 s) and extension (72°C for 1 min), followed by a final extension period of 10 min at 72°C before termination. PCR was carried out in a 20 μL total volume and included 1 × PCR buffer, 1.25 mM $MgCl_2$, 0.25 mM dNTP, 1 U Taq polymerase, 0.5 μM forward and reverse primers and 1 μL cDNA. The PCR products were subjected to electrophoresis in 1.5% agarose gel. The size of each PCR product was established by comparing with a 100-base step DNA ladder. Quantification of PCR products was performed by densitometric analysis of SYBR Safe-stained gels using a gel documentation system and Fiji analysis software. For each sample treatment, the integrated density value obtained for the target gene-specific band was divided by the signal obtained for the *EF1α* band, producing a relative mRNA abundance value. Integrated density values for the *EF1α* bands did not change significantly with treatment. The experiment was repeated at least 3 times for each gene. Results are presented as relative intensity ± standard error of the mean (SEM) of *n* trials.

ZO-1 Immunofluorescence Analysis

Three DPF *Tg (kdrl*: mcherry) larvae were exposed to LPS (100 μg/mL) by static immersion for 6 h at 28.5°C. Control larvae were exposed to embryo media. Embryos were fixed overnight at 4°C in 2% paraformaldehyde (PFA) in PBST (phosphate-buffered saline + 0.1% Tween 20). Embryos were then washed 4 times for 5 min in PBST at room temperature (RT) and permeabilized for 30 min at RT in PBST + 0.5% TritonX-100. Embryos were then blocked in PBST + 0.1% TritonX-100 + 10% normal goat serum (NGS) + 1% BSA for 2 h at RT. Embryos were incubated with primary antibodies (rabbit anti–ZO-1 mid; Invitrogen #40 2200) in blocking solution (1:200) overnight at 4°C. Embryos were then washed 6 times for 20 min in PBST at RT and incubated with the secondary antibody (goat anti-rabbit IgG Alexa fluor 488; 1:1000) in blocking solution for 2 h at RT. Embryos were finally washed 3 times for 10 min in PBST at RT and mounted in 4′,6-diamidino-2-phenylindole (DAPI) Vectashield. Images were taken with a Zeiss confocal microscope. An average of 3 trials with 4–6 larvae/treatment were used to obtain quantitative data.

Measuring Activation of Immune Cells and ROS Production

To visualize neutrophil activation and transmigration, 3 DPF *Tg (mpx*: GFP) larvae were exposed to LPS (100 μg/mL) by static immersion for 4 h at 28.5°C and imaged using a Leica fluorescence microscope (n = 7/treatment). To visualize the role played by neutrophils and macrophages in LPS-induced tissue damage, 3 DPF *Tg* (*coro1a*: eGFP; *lyz*: Dsred) double-transgenic larvae (macrophages display green fluorescence, while neutrophils display both green and red fluorescence) (24) were exposed to LPS (100 μg/mL) by static immersion for 6 h at 28.5°C and imaged using a Leica fluorescence microscope (n = 7/treatment). Neutrophil and macrophage numbers were counted using Fiji analysis software.

ROS production was visualized using 2′, 7′-dichlorodihydrofluorescein diacetate (DCFH-DA; Sigma-Aldrich), a ROS

Table 1. Primer pairs used in this study

Gene ID	Primer sequences (5′-3′)	Temp (°C)	Amplicon size (bp)
VE cadherin	Fwd: TGACGAGGAGGGCGGAGGAG Rev: AGGTCCCACACTGGGCCGAA	58	100
Occludin a	Fwd: TACCATTACTGCGTGGTGGA Rev: TCACTCTGCGCCATAAGATG	58	154
Occludin b	Fwd: TATGTTTGCCTGCGTAGCTG Rev: CGTATCCGTAGCCTCCCATA	58	182
Claudin 5a	Fwd: GGTCATCTCCTCGGTCTTGA Rev: GCACCTGCGGGTTATAGAAG	58	206
Claudin 5b	Fwd: CTCAATGCACCAATTGCATC Rev: TTTTTGGCGTAGGGAACTTG	58	166
Claudin 2	Fwd: CAACACCCTCCTGGGACTAA Rev: GCCAACTCCAGCTACTTTGG	58	163
ZO-1	Fwd: CACGAGACAAACTGGCAAGA Rev: TCCAGCACTGCATGCTTATC	58	178
IL-1	Fwd: TGGACTTCGCAGCACAAAATG Rev: GTTCACTTCACGCTCTTGGATG	58	150
IL-6	Fwd: AGACCGCTGCCTGTCTAAAA Rev: TTTGATGTCGTTCACCAGGA	58	136
TNF	Fwd: GCTGGATCTTCAAAGTCGGGTGTA Rev: TGTGAGTCTCAGCACACTTCCATC	58	138
IL-8l1	Fwd: GTCGCTGCATTGAAACAGAA Rev: CTTAACCCATGGAGCAGAGG	58	158
IL-8l2	Fwd: CTACCGAGACGTGGGTGATT Rev: GCTCGGTGAATGGTCATTTT	58	140
IL-10	Fwd: ATTTGTGGAGGGCTTTCCTT Rev: AATGGGAGTTGCAAAACTGG	60	127
HMGB1	Fwd: AGAGGAGGAGGATGACGAGTAG Rev: GGACGAACACAGATGACACTTC	60	232
TLR4a	Fwd: TGCAAAGGCTTGTTCTTGTG Rev: TGAAGGTGGTCATGAATGGA	60	138
TLR4b	Fwd: CTGTGTTGCGAGAGATTGGA Rev: AGGCAGCTAGCAGATGAAGC	60	120
MyD88	Fwd: TAAACGGCTAATCCCTGTCG Rev: TCGAGTCCAGAACCAGACCT	60	118
EF1α	Fwd: GATGCACCACGAGTCTCTGA Rev: TGATGACCTGAGCGTTGAAG	58	158

indicator (n = 4/treatment). Wild-type zebrafish were exposed to LPS (100 μg/mL) by static immersion for 5 h at 28.5°C and then incubated along with 100 μM DCFH-DA for 1h at 28.5°C in the dark, and washed 3 times for 5 min with embryo water. DCFH-DA diffuses into cells and is deacetylated by cellular esterases to nonfluorescent DCFH, which is rapidly oxidized to highly fluorescent 2′, 7′-dichlorofluorescein by ROS. The fluorescence intensity is proportional to the ROS level within the cell cytosol. To demonstrate that the effects observed on ROS production are LPS-specific, an LPS dose response with the resultant changes in ROS production was also performed. Wild-type zebrafish were exposed to different LPS concentrations (0, 25, 50, 75 and 100 μg/mL; n = 3/treatment) by static immersion for 5–6 h at 28.5°C and then incubated along with 100 μM DCFH-DA for 1 h at 28.5°C in the dark, and washed 3 times for 5 min with embryo water. Photographs were acquired using a Leica DFC 300-FX camera and a Leica fluorescence microscope, and were processed with Fiji analysis software.

Corrected total fluorescence (CTF) was calculated using the following formula:

CTF = integrated density – (area of selected cell × mean fluorescence of background readings)

Measuring Circulatory Defects

To visualize LPS-induced changes in circulation, 3 DPF *Tg* (*flk1*: GFP; *gata-1*: Dsred) double-transgenic larvae were exposed to LPS (100 μg/mL) by static immersion for 6 h at 28.5°C and imaged using a Leica fluorescence microscope (an average of 3 trials with 7 larvae/treatment). Control larvae were exposed to embryo media. Results were validated using o-dianisidine (OD) staining technique for hemoglobin. Briefly, larvae that were previously fixed in 4% PFA after LPS treatment were washed in PBST and then incubated for 6 min in the dark in o-dianisidine (OD) staining solution (10 mL solution contains 6 mg OD, 4 mL EtOH, 100 μL 1M sodium acetate and 5.9 mL water). The larvae were then washed 3 times for 5 min in PBST and imaged using a brightfield microscope.

To measure LPS-induced narrowing of blood vessels, the diameter of the dorsal aorta (directly above the tip of the yolk extension) was measured in pixel distance using a Leica fluorescence microscope, and then converted to μm using Fiji analysis software (n = 5–8/treatment).

Measuring Thrombocyte Aggregation

To visualize thrombocytes, the equivalent of platelets in humans (recruitment, clumping and possibly the formation of microvascular thrombi), 3 DPF *Tg (CD41*: GFP) larvae were exposed to LPS (100 μg/mL) by static immersion for 6 h at 28.5°C and imaged using a Leica fluorescence microscope (an average of 3 trials with 5–7 larvae/treatment).

Characterizing the Immunosuppressive State as Seen in Sepsis

To characterize the immunosuppressive state commonly observed in the later stages of sepsis, neutrophil numbers were counted at 6–7 h post-LPS treatment. Three DPF *Tg (mpx*: GFP) larvae were exposed to LPS (100 μg/mL) by static immersion for 6–7 h at 28.5°C and imaged using a Leica fluorescence microscope

(n = 7–12/treatment). Transcript levels of a late mediator of inflammation, *HMGB1* (25), were also determined by quantitative real-time PCR as described in the previous sections.

LPS Signaling in the Zebrafish Sepsis Model-Involvement of TLR4, MyD88 and NFκB

Transcript abundance of *TLR4a, TLR4b* and *MyD88* was determined through quantitative real-time PCR as described in the previous sections. NFκB protein expression and nuclear translocation were visualized through whole-embryo immunofluorescence using a modified protocol from Encinas *et al.* (26). Briefly, 3 DPF larvae were exposed to LPS (100 μg/mL) by static immersion for 2 h at 28.5°C. Control larvae were exposed to embryo media. Embryos were fixed overnight at 4°C in 2% PFA in PBST. Embryos were then washed 4 times for 5 min in PBST at RT and permeabilized for 30 min at RT in PBST + 0.5% TritonX-100. Embryos were then blocked in PBST + 0.1% TritonX-100 + 10% NGS + 1% BSA for 2 h at RT. Embryos were incubated with primary antibody (NFκB/p65 [Rel A] Ab-1, rabbit polyclonal antibody; RB-1638-P0) in blocking solution (1:200) overnight at 4°C. Embryos were then washed 6 times for 20 min in PBST at RT and incubated with the secondary antibody (goat anti-rabbit IgG Alexa fluor 488; 1:1000) in blocking solution for 2 h at RT. Embryos were finally washed 3 times for 10 min in PBST at RT and mounted in DAPI Vectashield. Images were taken with a Zeiss confocal microscope. An average of 3 trials with 3–4 larvae/treatment were used to obtain quantitative data.

Validating the Utility of the Zebrafish Sepsis Model for High-throughput Drug Screening Applications

Small-molecule drug libraries, which were assembled in-house, along with appropriate positive and negative controls, were initially dissolved in 100% dimethyl sulfoxide (DMSO) to a concentration of 10 mg/mL, and further diluted with nuclease-free water. Three DPF wild-type zebrafish larvae were co-incubated with LPS (100 μg/mL) and the small-molecule library (final drug concentration of 1μg/mL; DMSO was <0.01%) overnight at 28.5°C in a 96-well setup (dark-walled plates with clear bottoms; 1 larvae/well; experiment repeated 3 times). Appropriate controls were also set up on the same plate. Screening was done using our in-house high-throughput robotic drug discovery platform. Initial screening involved 96 small molecules (MW 250–500) targeting epigenetic regulators, immune modulators and their analogs (Life Chemicals). These molecules satisfy Lipinski's "rule of five" as well as Veber criteria and dissimilarity evaluation.

The three primary readouts used in our high-throughput screens were: (1) the ability of the small molecule to improve survival, (2) the ability of the small molecule to rescue LPS-induced vascular leakage and the resulting tail fin edema (observed through brightfield microscopy) and (3) the ability of the small molecule to rescue LPS-induced systemic ROS production (see protocol above); imaging and quantification were done using the ImageXpress Ultra confocal high-content analysis system (Molecular Devices).

To further test the effects of fasudil on LPS-induced mortality, vascular leakage and ROS production, 3 DPF zebrafish larvae were coincubated with LPS (100 μg/mL) at different concentrations of fasudil (0.01–75μM) to obtain the EC50 of the drug relative to survival (treatment was conducted using triplicate groups of 10 larvae per treatment). FITC-dextran injections (an average of 3 trials of 10 larvae/treatment) and ROS production assays (see protocols above; an average of 3 trials of 3 larvae/treatment) were also used to assess the ability of fasudil to rescue LPS-induced vascular leakage and ROS production.

Statistical Analysis

Data are shown as mean ± SEM. *T* tests (for control versus LPS experiments) and two-way analysis of variance with Tukey post hoc test (for drug rescue experiments) were used for statistical comparisons to determine treatment differences. Statistical analysis was performed on either raw or transformed data when necessary to meet normality and equal variance assumptions. A probability level of $P < 0.05$ was considered significant. All statistical analyses were performed using Graph Pad Prism software.

All supplementary materials are available online at www.molmed.org.

RESULTS

Tail Fin Edema and Mortality Caused by Exposure to LPS

Three DPF zebrafish larvae exposed to LPS showed a dose-dependent increase in mortality (Figure 1A). While lower concentrations of LPS (25 or 50 μg/mL) did not cause mortality in the first 24 h, 5% of larvae in the 50 μg/mL group developed a swollen pericardial sac (Figure 1B). Exposure to moderate to high LPS doses of 75 or 100 μg/mL resulted in 40% and 93% mortality, respectively. Pericardial swelling was seen in larvae exposed to 50 and 75 μg/mL LPS. While only 7.5% of the larvae in the 75 μg/mL group developed tail fin edema and tissue damage, 92.5% of larvae exposed to 100 μg/mL of LPS developed tail fin damage and edema. Moreover, the tail fin edema and damage observed in the larvae exposed to 100 μg/mL of LPS worsened over time (Figures 1C, D). Following LPS exposure, the highest dose of 200 μg/mL resulted in hemorrhagic pericardium and a high mortality rate of 37% by 2 h and 100% by 7 h. Based on the mortality dose response to LPS, all subsequent experiments were performed using an LPS dose of 100 μg/mL due to the fact that this dose resulted in a tail phenotype suitable for phenotype-based drug screening and also mortality if no intervention was made.

LPS-Induced Vascular Leakage in Zebrafish Larvae

Injection of quantum dots (QD605) provided bright vital labeling showing increased vascular leakage in 47%

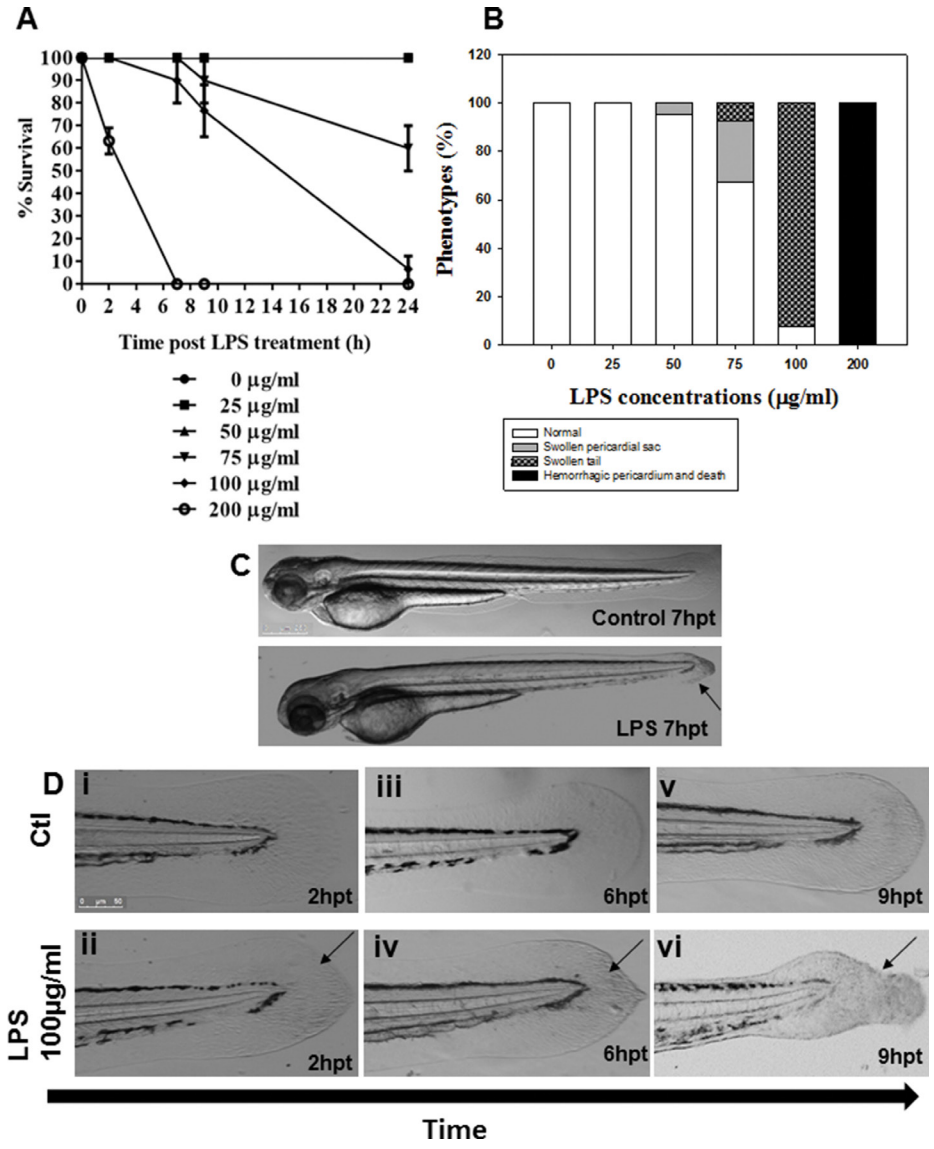

Figure 1. LPS induces mortality and tail fin edema in zebrafish larvae. (A) LPS dose-dependently induces mortality in 3 DPF zebrafish larvae (an average of 3 trials with 10 larvae per treatment). (B) The different concentrations of LPS tested show different phenotypes in these larvae (40 larvae/LPS concentration at 6 h post LPS exposure). A predominant phenotype is the LPS-induced tail fin edema and tissue damage observed in the larvae treated with 100 µg/mL LPS. (C, D) This phenotype worsens over time and results in mortality if untreated.

of zebrafish larvae (*Flk1*: GFP) following exposure to LPS (100 µg/mL) (Figures 2A, B). The most pronounced leakage of QD was observed in the region directly above the tip of the yolk extension (Figure 2A), along the posterior cardinal vein (PCV). Since QD are relatively large (approximately the size of a macromolecule ~15–20 nm), smaller leaks could not be discerned using this method. To address this, we used green-labeled FITC-dextran with a molecular weight of 4 KD (~14 Angstroms) to demonstrate LPS-induced vascular leakage through the intersegmental vessels (ISVs) and accumulation of FITC-dextran at the tip of the tail, which corresponded to the edema and tissue damage seen in the tail fin (Figure 2C). Time-lapse imaging of LPS-induced vascular leakage after FITC-dextran injections enabled real-time visualization of *in vivo* vascular leakage (see Supplemental Data). Injection of FITC-dextran detected vascular leakage in 97% of the larvae and was established as a more reliable method than quantum dot injections in detecting LPS-induced vascular leakage (Figure 2D).

LPS Alters Expression and Distribution of Cellular Junction Proteins

Following endotoxemia, vascular leakage is thought to result from the direct action of microbial or/and host factors on endothelial cells and/or their tight and adherens junctions (TJs and AJs, Figure 3A). While AJs are fundamental to tissue integrity, TJs are associated with barrier function (27). Exposure of zebrafish larvae to 100 µg/mL LPS significantly decreased the transcript levels of TJ proteins *occludin A* (2.7-fold; Figure 3B), *occludin B* (2.4-fold; Figure 3C), *claudin 5a* (1.9-fold; Figure 3D) and *claudin 5b* (1.8-fold; Figure 3E), increased the expression of *claudin 2* (four-fold; Figure 3F), and had no effect on the transcript levels of the AJ protein *VE cadherin* (Figure 3G). LPS also caused a significant decrease (2.6-fold; Figure 3H) in the transcript levels of *ZO-1*, which is a scaffold junction protein associated with transmembrane TJ proteins, the cytoskeleton and signal transduction molecules (28). ZO-1 protein expression was also markedly reduced (Figure 3I) and appeared to be disrupted/fragmented at the site of LPS-induced tail edema and tissue damage (Figure 3J).

LPS Induces Extravascular Migration of Neutrophils and Macrophages

Through the use of transgenic zebrafish lines with fluorescently labeled neutrophils and macrophages, we quantified leukocyte migration out of circumscribed vessels. Neutrophils were quiescent in an untreated 3 DPF larva, located primarily in the dorsal aorta (DA; Figure 4Ai).

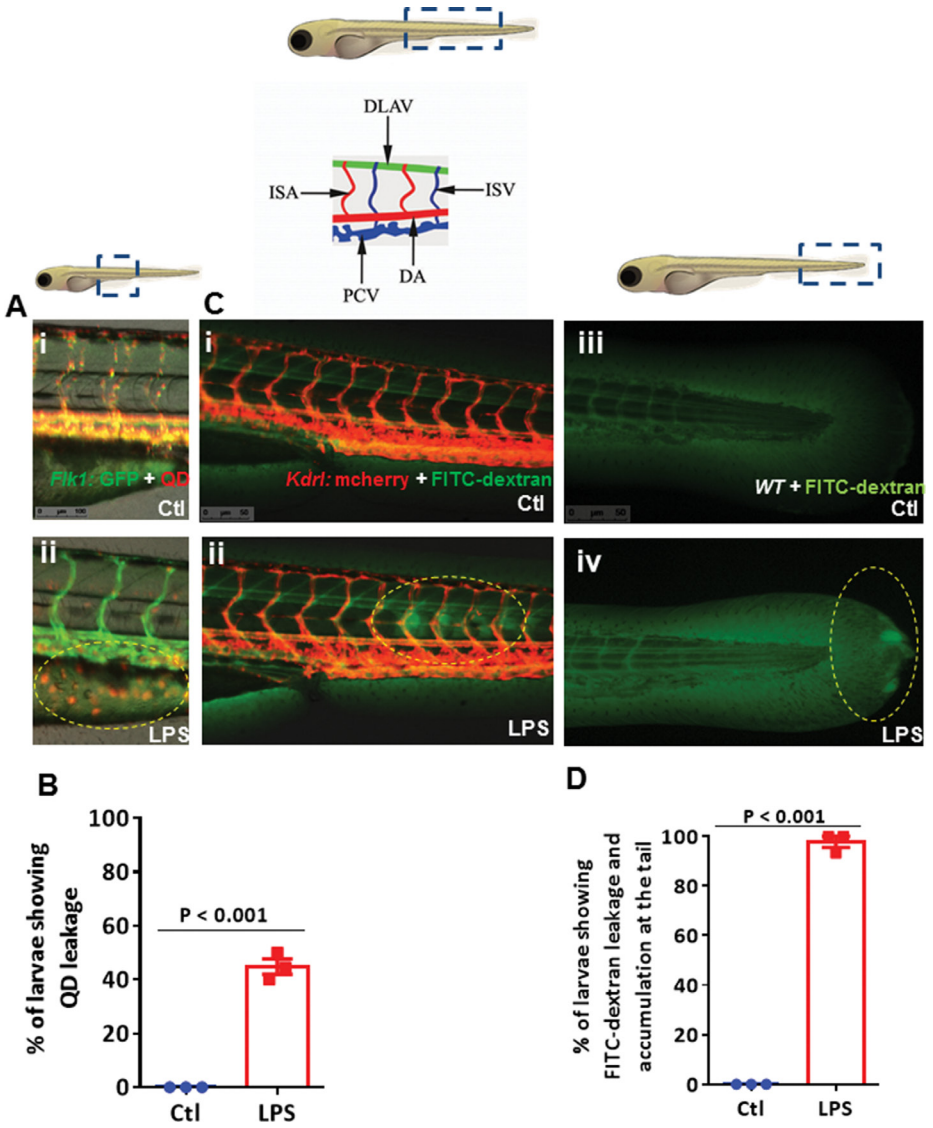

Figure 2. Use of transgenic zebrafish lines and microangiography contrast agents help visualize vascular leakage. The use of transgenic zebrafish lines (*Flk1:* GFP and *Kdrl:* mcherry) together with injection of microangiography contrast agents like QD605 and FITC-dextran, respectively, help visualize LPS-induced vascular leakage in 3DPF zebrafish larvae. (A, B) While QD605 are useful in detecting major leaks at the region below the PCV (an average of 3 trials of 9–14 larvae per treatment), (C, D) FITC-dextran is better suited for visualizing minor leaks through the ISVs and the subsequent accumulation of the leaked out dextran at the tail fin (an average of 3 trials of 10–15 larvae per treatment). DLAV: dorsal longitudinal anastomotic vessel; ISA: intersegmental artery; ISV: intersegmental vein; PCV: posterior cardinal vein; DA: dorsal aorta

Exposure to LPS resulted in migration of neutrophils from the DA into the interstitial space during the early stages of inflammation (Figure 4Aii, B). LPS also induced migration of macrophages out of the intravascular space into extravascular fluid in edematous tails (Figures 4C, D).

Increased ROS and Inflammatory Mediator Expression Following Exposure to LPS

Their fast diffusion and versatile biological activity make ROS good candidates to determine the presence and degree of diffuse injury and wound-to-leukocyte signaling. LPS induces increased ROS production in a dose-dependent manner (Supplementary Figure S1). Following LPS exposure, there was a rapid and marked increase in ROS production (34-fold) in zebrafish larvae (exposed to 100 μg/mL LPS) compared with controls (Figures 5A, B). Increased ROS production in the tails of LPS-treated larvae corresponded with the observed tail and tissue damage. Increased interstitial edema and ROS production were further associated with a modest increase in the expression of key proinflammatory cytokines and a larger increase in the expression of antiinflammatory cytokines *IL-1* (1.2-fold; Figure 5C), *IL-6* (1.3-fold; Figure 5D), *TNF* (1.6-fold; Figure 5E), *IL-8l1* (1.5-fold; Figure 5F), *IL-8l2* (1.3-fold; Figure 5G) and *IL-10* (5.5-fold; Figure 5H).

LPS Induced Narrowing of Blood Vessels, Reduced Blood Flow and Thrombocyte Aggregation

Upon exposure to LPS, >86% of 3 DPF larvae demonstrated reduced microvascular circulation in brain capillaries, largely in the central arteries, observed through the use of transgenic zebrafish lines and hemoglobin staining (Figures 6A, B). We also observed poor and defective circulation through the DA and PCV (Figure 6C), accompanied by narrowing of the DA (Figure 6D). In >80% of larvae, we also observed increased thrombocyte clumping in the CCV and the caudal region of the embryo between the DA and the PCV compared with controls, which showed a few circulating thrombocytes in the caudal region of the zebrafish larvae (Figures 6E, F).

Reduced Neutrophil Numbers and Increased HMGB1 Expression Suggest an Immunosuppressive State in the Zebrafish Sepsis Model

We observed lower neutrophil numbers (Supplementary Figures S2A, S2B) and increased expression (2.5-fold) of *HMGB1* (Supplementary Figure S2C)

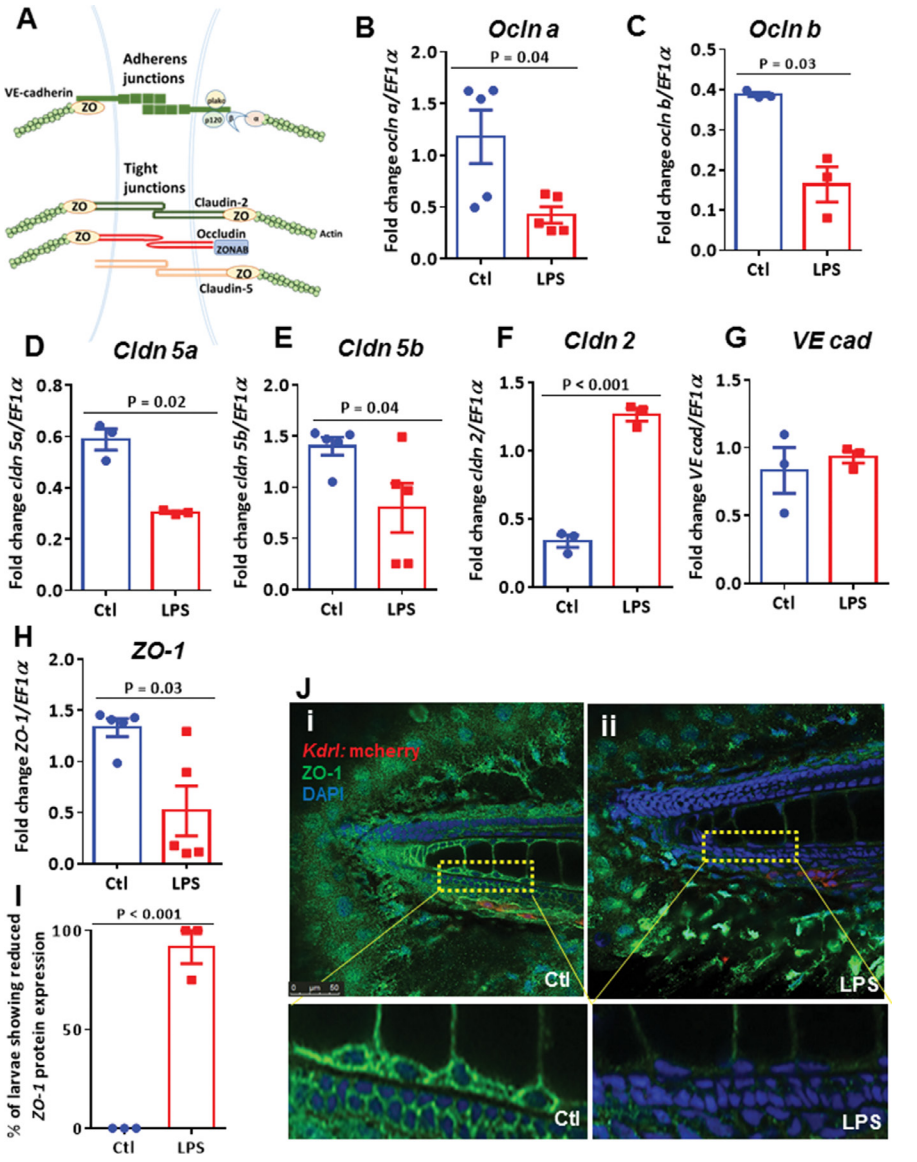

Figure 3. LPS induces changes in junction protein expression in zebrafish. (A) A schematic representation of the various cellular junction proteins. LPS reduces the transcript abundance of (B) *occludin a*, (C) *occludin b*, (D) *claudin 5a* and (E) *claudin 5b*, (F) increases the transcript abundance of *claudin 2* and (G) has no effect on the transcript abundance of *VE cadherin*. LPS treatment also (H, I) decreased the transcript and protein levels of ZO-1 and (J) caused disorganized patterning and increased fragmentation of ZO-1 protein. For experiments on transcript levels, an average of 3–5 trials was used, each with a pool of 20 larvae/treatment. For the immunohistochemistry experiments, an average of 3 trials with 4–6 larvae/treatment were used to obtain quantitative data.

during the later stages of inflammation (6–7 h post LPS treatment) in our zebrafish sepsis model, suggesting an immunosuppressive state in this model which mimics that observed in clinical sepsis.

LPS Signaling in the Zebrafish Sepsis Model Involves Upregulation of NFκB, Nuclear NFκB Translocation and Increased *MyD88* Expression

LPS-induced endotoxemia in the zebrafish sepsis model was mediated through NFκB and MyD88 signaling. The NFκB fluorescence was localized mainly in the cytoplasm of control zebrafish larvae. However, the fluorescence appeared also in the nuclei and its intensity was increased in LPS-treated larvae (2 h post LPS treatment), suggesting both induced translocation and new synthesis of zebrafish NFκB (Supplementary Figures S3A, S3B). This was also associated with increased *MyD88* expression (2.8-fold; Supplementary Figure S3C), but no changes in *TLR4* transcript levels (Supplementary Figures S3D, S3E).

Evaluation of Endotoxin-Induced Parameters for High-throughput Drug Screening

We established a protocol using healthy 3 DPF larvae distributed in 96-well plates and exposed to LPS and different drug libraries assembled in-house for 14–16 h to detect the effect of candidate chemical compounds on LPS-induced mortality, vascular leakage (characterized by tail fin edema) and ROS production. Surrogate markers of endotoxemia severity were selected as the basis for our phenotype screen, based on reproducibility, ease of detection, visualization, quantification and relevance to the pathophysiology of sepsis. Various lead candidates reduced primary (tail fin edema and ROS production) and secondary (mortality) outcome markers of LPS-induced injury. From our preliminary screen of 96 proprietary small-molecule compounds, 10 compounds were identified to rescue all three phenotypes tested for. One of the hits identified was fasudil (Figures 7A, B), a drug known to rescue LPS-induced vascular leakage in murine models of experimental sepsis (29). Response to fasudil was used to validate the utility of our model for identifying novel modifiers of mortality, vascular leak and ROS production. Further testing of this drug in zebrafish showed that fasudil protected against LPS-induced mortality in a dose-dependent manner, with an EC50 of 3.852 μM for survival (Figure 8A). Additionally, while all larvae that were

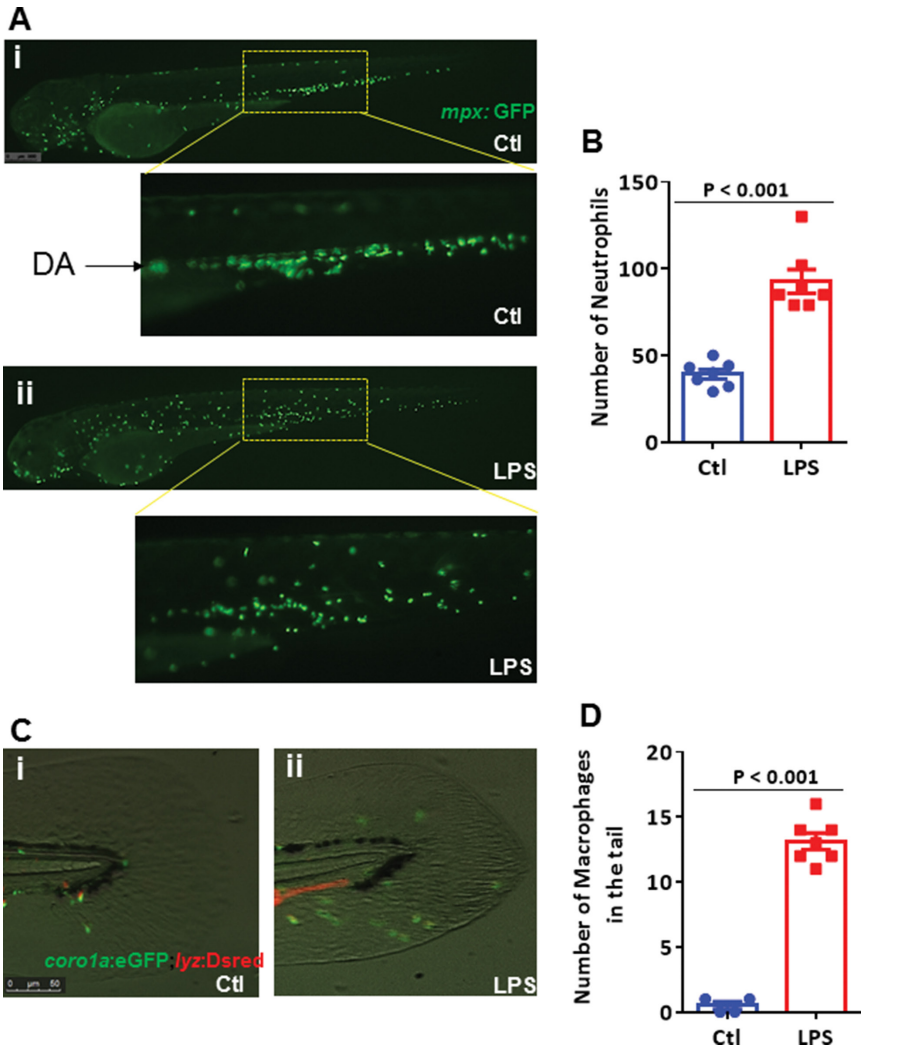

Figure 4. Immune cell migration in endotoxemic zebrafish. (A, B) LPS exposure in *mpx:* GFP larvae causes extravascular migration of neutrophils from major blood vessels, namely the dorsal aorta (n = 7/treatment). (C, D) LPS exposure in *coro1a*:eGFP;*lyz*:Dsred also induces migration of macrophages out of the intravascular space into extravascular fluid in edematous tails (n = 7/treatment). DA: dorsal aorta

exposed to LPS and received vehicle drug treatment showed tail edema and swelling accompanied by vascular leakage and accumulation of FITC-dextran at the tail, 88% of the larvae treated with fasudil and LPS showed a complete rescue of the tail phenotype and FITC-dextran leakage (Figures 8B, C). Fasudil on its own had no effect on vascular leakage and no toxic effect on zebrafish larvae. Fasudil also rescued LPS-induced ROS production at the tail (Figures 8D, E). Interestingly, the LPS-treated larvae showed reduced ROS in the swim bladder compared with controls, fasudil-treated and LPS + fasudil-treated larvae (Figure 8F).

DISCUSSION

Here we establish a novel zebrafish model of endotoxin-induced inflammation and injury that recapitulates major physiological and cellular features of human sepsis. Exposure of zebrafish larvae to high-dose LPS resulted in vascular leakage, leading to tail fin edema and tissue damage, which worsened over time and, in the absence of intervention, was associated with high mortality. The tail phenotype was also associated with increased quantum dot and dextran leakage from intravascular into interstitial spaces, primarily along the tail. Loss of vascular permeability was further associated with reduced expression of tight junction protein genes, increased expression of the water pore gene claudin 2, increased infiltration of macrophages and neutrophils, and increased cytokine expression and ROS production. LPS exposure was also associated with constriction of the dorsal aorta, with evidence of impaired blood flow to the brain and increased platelet aggregation, indicative of both vasoconstriction in large arteries and platelet dysfunction.

PRRs, their downstream signaling pathways and innate immune effector mechanisms are conserved between humans and zebrafish (9,13). LPS is a major constituent of the outer membrane of gram-negative bacteria. It is a potent immunostimulant known to induce organ dysfunction, vasoplegia and even death in vertebrate models (30). Moreover, most cases of human sepsis are associated with bacterial infection, and gram-negative bacteria are often implicated in the pathogenesis of severe sepsis and septic shock (31). Although recent studies have used microinjection of bacterial extracts to induce inflammation and sepsis-like pathophysiology in zebrafish (32), we used a simpler technique (waterborne exposure to LPS), which is better suited for high-throughput drug screening.

Increased vascular permeability contributes to the pathophysiology of sepsis, as well as multiple other disease states. A greater understanding of endotoxin-induced interstitial edema formation may provide fundamental insights into the mechanisms of loss of barrier function. Microinjection of microangiography contrast agents like quantum dots (QD605) and FITC-dextran can enable direct visualization of changes in vascular permeability in real time and subsequent evaluation of drugs targeting vascular permeability *in vivo* (23). We observed in real time widespread loss of vascular

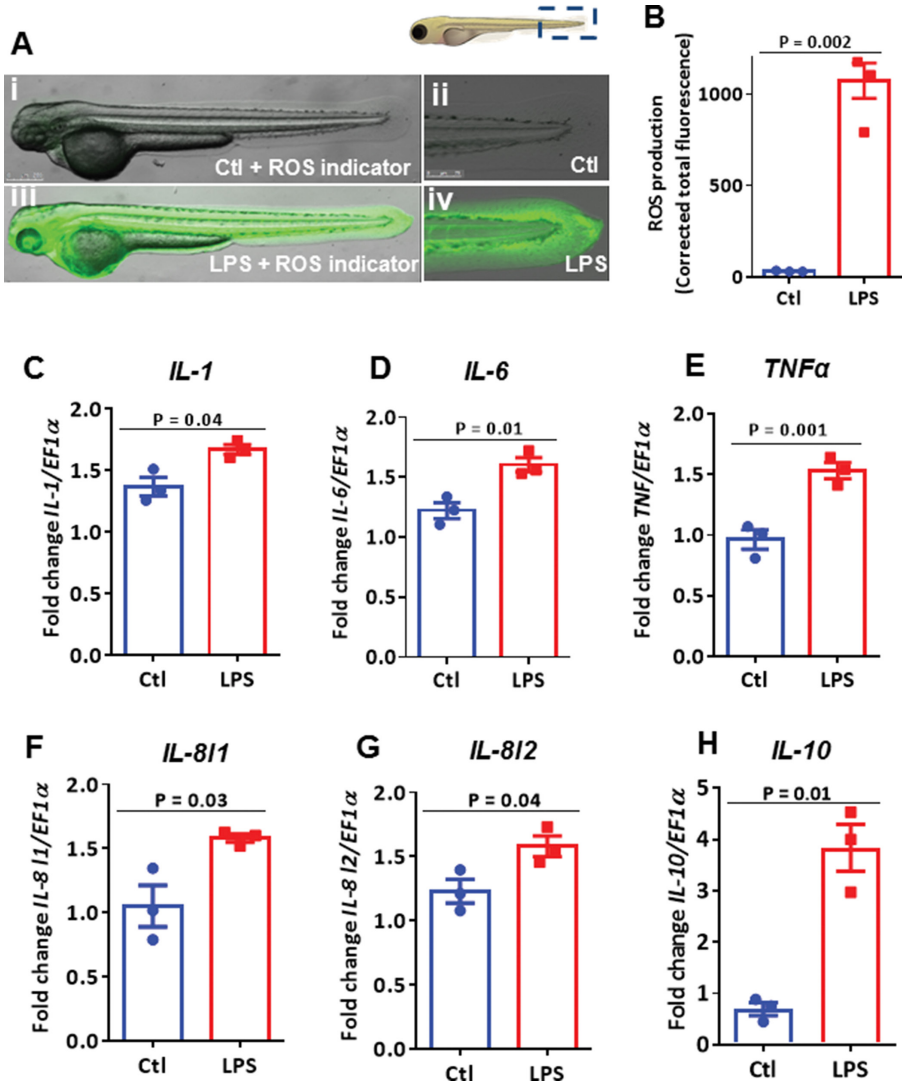

Figure 5. LPS induces ROS production and increased proinflammatory and antiinflammatory cytokine expression in zebrafish. (A, B) LPS exposure leads to systemic production of ROS (n = 4/treatment) and an increase in the transcript levels of key proinflammatory cytokines (C) *IL-1β*, (D) *IL-6*, (E) *TNFα* and (F, G) *IL-8* and (H) the antiinflammatory cytokine *IL-10*. For experiments on transcript abundance, an average of 3 trials was used, each with a pool of 20 larvae/treatment.

integrity and a consequent increase in vascular leakage in our LPS-induced zebrafish sepsis model. While QD605 injections helped to detect major leaks, FITC-dextran injections helped to visualize minor leaks in the ISVs and also the accumulation of leaked FITC-dextran at the tail fin. This corresponded with the tail fin edema seen in these larvae.

The breakdown of barrier integrity has been attributed, at least in part, to the altered expression and distribution of cellular junction proteins (18,33). Increased vascular permeability in our model was accompanied by reduced expression of tight junction proteins occludin a and b, claudin 5a and b, and their intracellular partner ZO-1. Though claudin 5 in zebrafish is considered to be more specific to endothelial cells, its expression is restricted to the central nervous system and hyaloid vasculature. In contrast, claudin 5b is expressed throughout the vascular system. Other tight junction proteins like occludin and many claudin family members are seen not only in endothelial cells but also in epithelial cells (34,35). In these cells, TJs help generate the primary barrier against the diffusion of solutes through the paracellular route (34).

It should be noted that we measured whole-body junction protein expression and made no distinctions between epithelial and endothelial junction proteins in our expression analyses. Our results are in line with studies in mouse sepsis models, which also show marked reductions in occludin and claudin 5 levels (36,37). Studies in septic mice have also shown decreased ZO-1 expression and disorganized patterning with greater fragmentation, similar to our findings in the zebrafish sepsis model (38). We also saw upregulation of claudin 2 expression, pore forming tight junction protein, known to be markedly upregulated in mouse polymicrobial sepsis models (37). Interestingly, we did not detect any significant differences in VE cadherin expression, though this AJ protein is widely implicated in regulating endothelial integrity and permeability. This discrepancy might be due to the fact that we measured total VE cadherin transcript levels, while most changes in VE cadherin–mediated endothelial permeability are a consequence of post-translational changes, namely VE cadherin phosphorylation and rapid internalization and cleavage, which do not necessarily reflect changes at the transcript level (39).

Expression of the proinflammatory mediators *IL-1*, *IL-6* and *TNF* and the two homologues of *IL-8* were moderately increased in zebrafish larvae exposed to pathological concentrations of LPS at 6 h post treatment (hpt). Cytokine levels are known to be temporally regulated in response to infection, and we might have missed the peak levels in proinflammatory cytokine expression typically observed in the first few hours following immune insult (40). Moreover, the significantly high expression of the antiinflammatory cytokine *IL-10* suggests

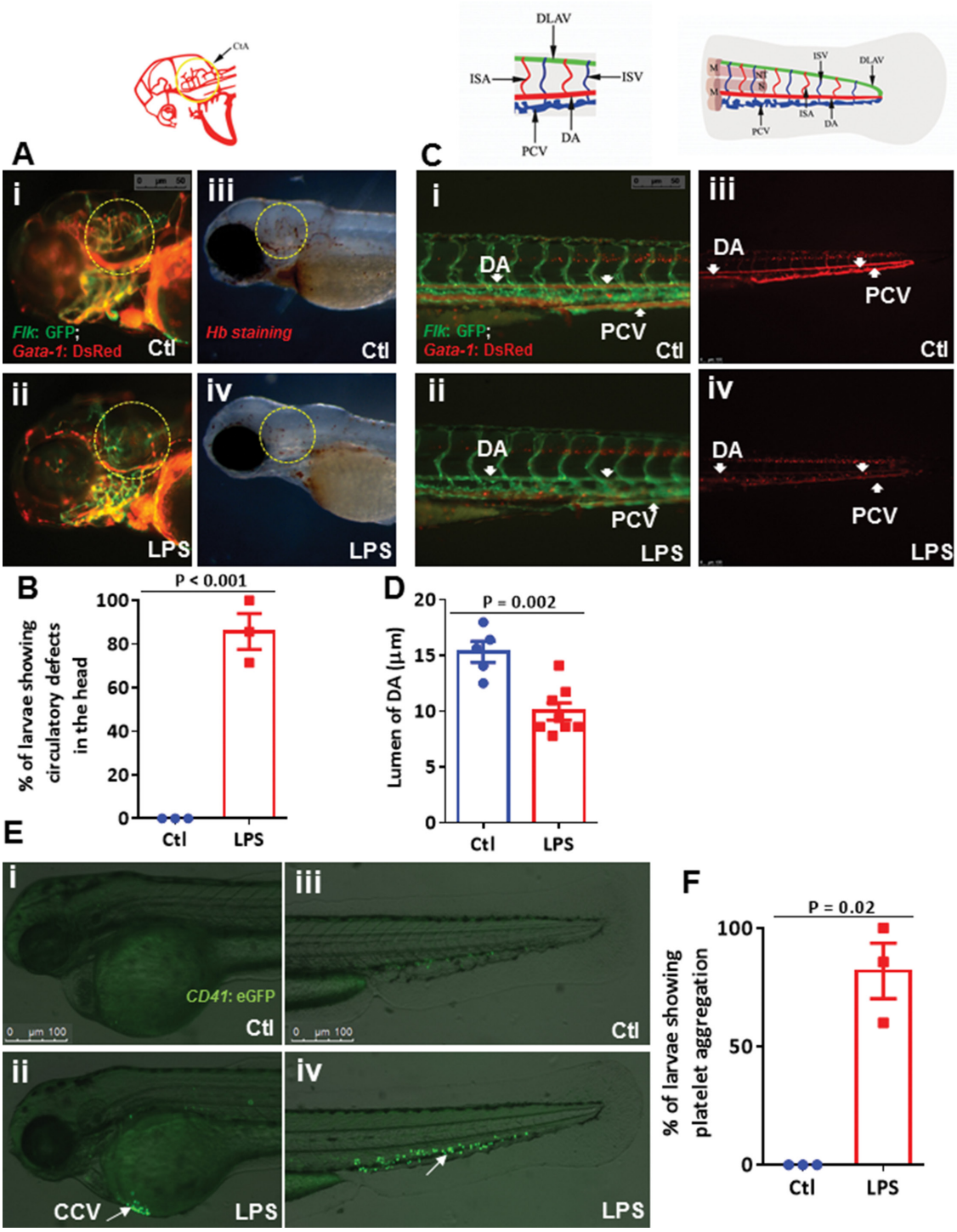

Figure 6. LPS induces blood flow abnormalities in endotoxemic fish. (A, B) LPS exposure in 3 DPF zebrafish larvae leads to marked changes in the microcirculation, characterized by reduced blood flow through the central arteries of the head (as observed through the use of transgenic zebrafish lines and Hb staining; an average of 3 trials with 7 larvae/treatment), microconstriction of the DA (n = 5–8/treatment) and (C, D) reduced circulation through the DA and PCV. (E, F) LPS-treated larvae also show an increased aggregation of thrombocytes in the CCV and major blood vessels, namely DA and PCV (an average of 3 trials with 5–7 larvae/treatment) CtA: central arteries; DLAV: dorsal longitudinal anastomotic vessel; ISA: intersegmental artery; ISV: intersegmental vein; PCV: posterior cardinal vein; DA: dorsal aorta; M: muscle; NT: neural tube; N: notochord; CCV: common cardinal vein.

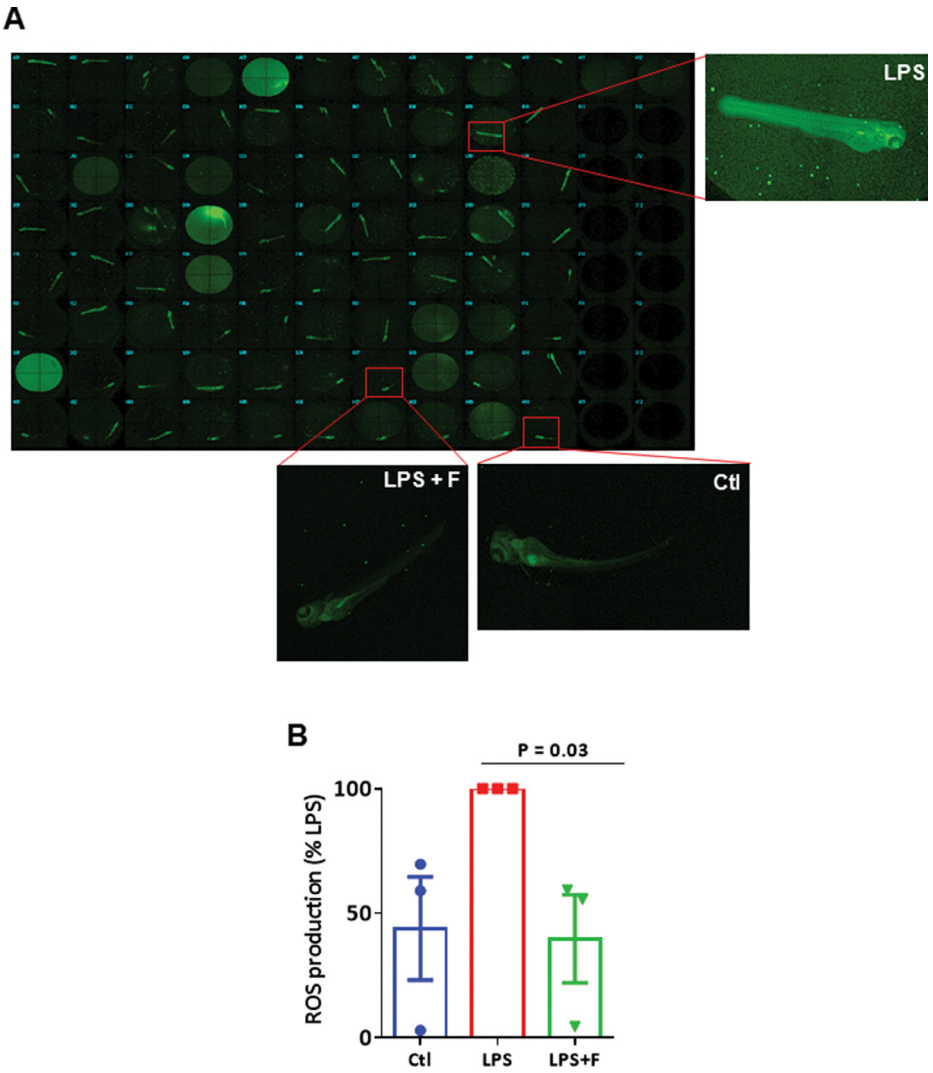

Figure 7. Identification of fasudil using a high-throughput drug screen. (A) A representative image of the 96-well readout for ROS production obtained from our in-house robotic drug screening platform is shown. (B) Fasudil, a lead hit identified using the screen, rescued LPS-induced ROS production, tail fin edema and mortality in our zebrafish sepsis model (n = 3).

progression to an immunosuppressed phenotype, often implicated as a cause of later secondary infections in sepsis (41). The cytokines and chemokines measured in this study are commonly used as measures of the teleost immune response and have been previously shown to be fairly conserved (sequence conservation and/or structural conservation) between zebrafish and mammals (16,42,43). However, many of the zebrafish cytokine genes have duplicated and diverged independently over the course of evolution, the functional implications of which are not entirely clear (44). In human, as well as in nonprimate models of endotoxemia and sepsis, these proinflammatory mediators have been shown to act synergistically to induce a shock-like state characterized by increased vascular permeability, severe pulmonary edema and hemorrhage (45). These cytokines and chemokines activate macrophages, promote neutrophil recruitment, activate coagulation pathways and amplify inflammatory cascades in an autocrine and paracrine manner (46). In our model, upregulation of proinflammatory mediators was associated with increased neutrophil and macrophage migration, accompanied by increased ROS production, especially in the tail. In sepsis, neutrophil accumulation in the vasculature and peripheral organs can lead to nonspecific cell and tissue damage in several organs, including lung, kidney, diaphragm, liver and intestine (47). Additionally, neutrophils also contribute to sepsis-associated blood coagulation and microvascular plugging through their binding to endothelial walls and the formation of platelet-leukocyte aggregates (47). Further studies will investigate the specific role of circulating versus parenchymal cells in the pathogenesis of endotoxin-induced tissue injury.

Microcirculation undergoes massive alterations during sepsis/septic shock. Local arteriolar constriction and increased endothelial permeability disrupt normal blood flow (48). We observed very little circulation through the brain capillaries in the zebrafish sepsis model. Shunting of flow may lead to slowing of capillary blood flow and, together with capillary obstruction caused by microthrombi, may decrease O_2 delivery to tissues and impair removal of CO_2 and waste products (48). We also observed reduced circulation through major blood vessels like the DA and PCV and a narrowing of the DA. This was accompanied by the aggregation of thrombocytes in the vasculature, which may be an indication of the formation of LPS-induced microvascular thrombi and microvascular plugging associated with sepsis (49), potentially leading to decreased tissue perfusion. Future mechanistic studies aimed at elucidating hemodynamic compromise associated with pathological exposure to LPS are currently under way.

Patients dying from sepsis also demonstrate a state of immunosuppression (50). This state of systemic immunosuppression not only results in a failure to eradicate primary infections, but also leads to the acquisition of lethal secondary infections. Immunosuppression in sepsis is associated with the exhaustion of immune cells and altered levels of immunomodulatory

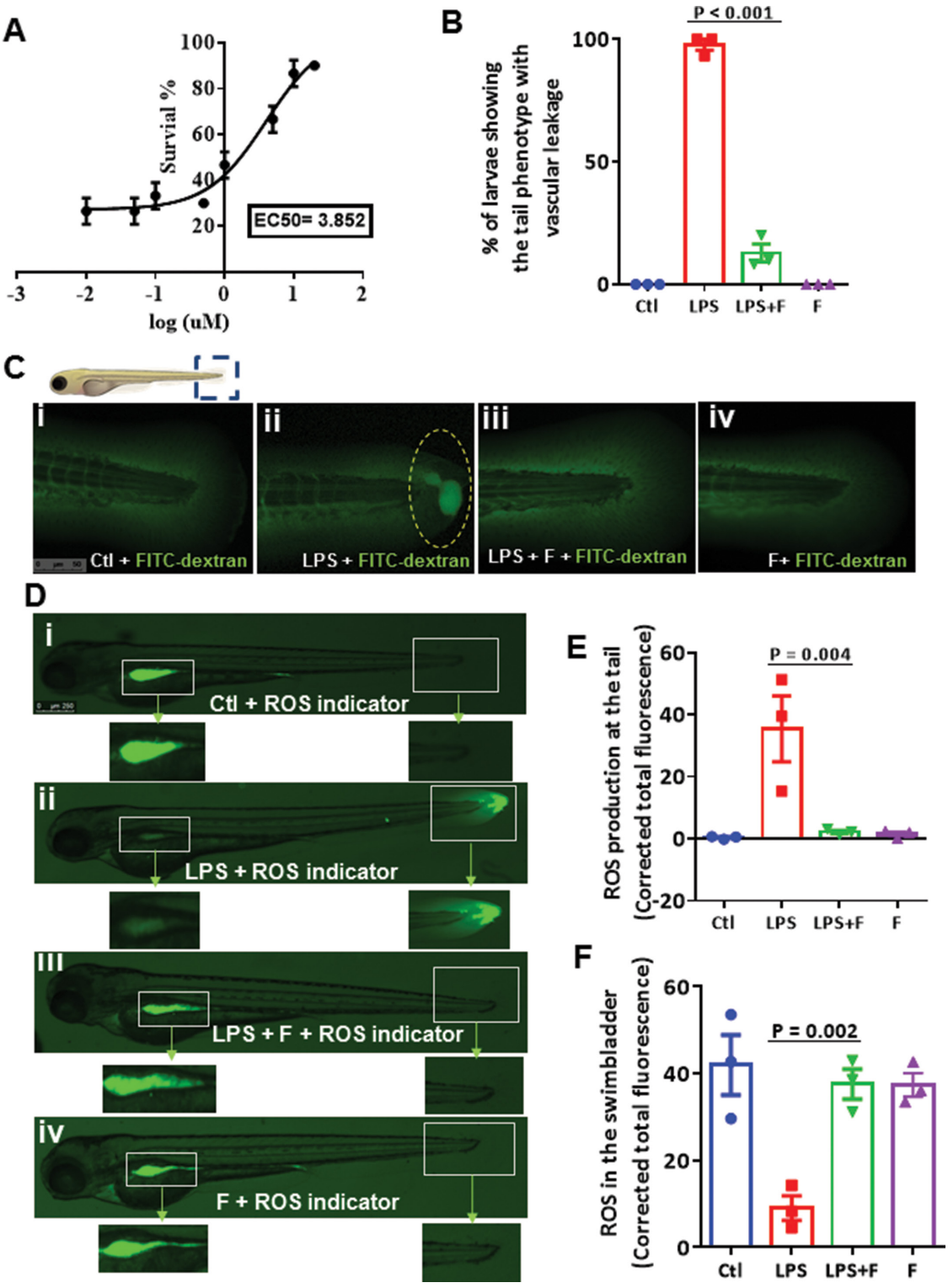

Figure 8. (A)Fasudil reverses LPS-induced vascular leakage and ROS production. Fasudil has an EC50 of 3.852 μM. (B, C) Fasudil mitigates LPS-induced vascular leakage and the resulting leakage of FITC-dextran and its accumulation at the tail fin (an average of 3 trials of 10 larvae/treatment). (D, E) Fasudil also rescued LPS-induced ROS production at the tail fin (an average of 3 trials of 3 larvae/treatment) and (F) LPS-induced reduction of ROS in the swim bladder (an average of 3 trials of 3 larvae/treatment).

molecules such as cytokines (50). Though we observed increased neutrophil extravasation in the early stages of inflammation in our model, neutrophil numbers were significantly reduced in the later stages of LPS-induced inflammation. This is in line with previous data showing marked decreases in neutrophil numbers in human patients with severe sepsis (51). It has been proposed that this reduction in neutrophil numbers might be due to a self-sacrificing mechanism of neutrophils against invading bacteria called "NETosis" (NET: neutrophil extracellular traps). In response to inflammatory stimuli, neutrophils extravasate from the circulation to infected tissues and initiate NETosis, whereby they release granule proteins, such as neutrophil elastase and myeloperoxidase, which serve to degrade virulence factors and kill bacteria. In the case of severe sepsis, many neutrophils are thus consumed for the elimination of bacteria (51). Although NETs are generally considered to be beneficial, excessive formation may also cause unintended injury to the host by activating platelets, leading to microvascular plugging. Reduced neutrophil numbers may also pave the way for secondary opportunistic infections.

HMGB1, primarily known for its role as a DNA-binding protein facilitating gene transcription, has now been recognized as a proinflammatory cytokine and a late mediator of inflammation (25). Interestingly, *HMGB1* expression was also markedly increased in our zebrafish sepsis model at the later stages of inflammation. HMGB1 accumulation in the late phase of sepsis in humans is known to play a major role in the development of postsepsis immunosuppression (52). Moreover, therapeutic blockade of HMGB1 in murine sepsis models has been shown to improve mortality (25). Whether the same hold true in zebrafish remains to be investigated.

The mechanisms underlying LPS signaling in teleosts is widely debated. Many teleosts lack a TLR4 receptor but still respond to LPS, underscoring the fact that LPS signaling in teleosts does not occur via the traditional TLR4 signaling pathways. We also did not see any changes in *TLR4* expression upon LPS stimulation. Nevertheless, we show here that recognition of LPS in our zebrafish sepsis model does require NFκB translocation and MyD88, similar to previous studies (13,26).

Using our zebrafish endotoxemia model, we have established a novel screening protocol to screen numerous compounds for antivascular leakage/anti-endotoxin properties. The three primary readouts used (rescue of mortality, rescue of the tail phenotype and rescue of ROS production) are very straightforward and do not require invasive procedures. One of the leads identified by this screen was fasudil, an inhibitor of the RhoA/Rho-kinase pathway, which has been implicated in loss of endothelial barrier function and increased vascular permeability associated with endotoxin-induced sepsis (53). Furthermore, fasudil has also been shown to rescue LPS-induced vascular leakage in mouse models (29).

Fasudil administration along with exposure to LPS reduced tail edema, dextran leakage and ROS production in zebrafish larvae. Interestingly, the larvae exposed to LPS showed reduced ROS production in the swim bladder compared with the other three groups. The swim bladder of fish is homologous to the tetrapod lung. In fish, this is primarily associated with hydrostatic functions (54,55). Oxygen is the main gas in the swim bladder, and the tissues of this organ are frequently exposed to constant hyperoxia, leading to increased production of ROS (56). This may explain the increased ROS production that we observed in control fish. Swim bladders are also known to act as oxygen reservoirs from which the blood can draw extra oxygen in times of need (55). This may explain the low ROS levels seen in the LPS-treated zebrafish larvae, suggesting that oxygen may be drawn from the swim bladder to compensate for LPS-induced hypoxia in different parts of the body and distant tissues.

CONCLUSION

In summary, administration of waterborne LPS to larval zebrafish recapitulates many phenotypic and cellular changes associated with human sepsis. These can be reliably visualized, quantified and reversed by administration of an antivascular leakage compound such as fasudil. Importantly, clinically relevant outcomes (such as mortality, vascular leakage and ROS production) can be utilized to screen various compounds on larval zebrafish using a high-throughput approach.

ACKNOWLEDGMENTS

We thank Koroboshka Brand-Arzamendi for the schematic diagrams/illustrations used in the paper, and for help with confocal imaging.

DISCLOSURE

The authors declare they have no competing interests as defined by *Molecular Medicine* or other interests that might be perceived to influence the results and discussion reported in this paper. Parts of this work have been previously presented in abstract form.

REFERENCES

1. Singer M, *et al.* (2016) The third international consensus definitions for sepsis and septic shock (sepsis-3). *JAMA.* 315:801–10.
2. Marshall JC. (2014) Why have clinical trials in sepsis failed? *Trends Mol. Med.* 20:195–203.
3. Bhatia SN, Ingber DE. (2014) Microfluidic organs-on-chips. *Nature Biotech.* 32:760–72.
4. Roses AD. (2008) Pharmacogenetics in drug discovery and development: a translational perspective. *Nat. Rev. Drug Discov.* 7:807–17.
5. Lieschke GJ, Currie PD. (2007) Animal models of human disease: zebrafish swim into view. *Nature Rev. Genet.* 8:353–67.
6. Howe K, Clark M, Torroja C, *et al.* (2013) The zebrafish reference genome sequence and its relationship to the human genome. *Nature.* 496:498–503.
7. Miscevic F, Rotstein O, Wen X-Y. (2012) Advances in zebrafish high content and high throughput technologies. *Comb. Chem. High Throughput Screen.* 15:515–21.
8. Gallardo VE, et al. (2015) Phenotype-driven chemical screening in zebrafish for compounds that inhibit collective cell migration identifies multiple pathways potentially involved in metastatic invasion. *Dis. Models Mech.* 8:565–76.
9. van der Vaart M, Spaink HP, Meijer AH. (2012) Pathogen recognition and activation of the innate immune response in zebrafish. *Adv. Hematol.* 2012:1–19.
10. Sunyer JO. (2013) Fishing for mammalian paradigms in the teleost immune system. *Nat. Immunol.* 14:320–26.

11. Stachura DL, Svoboda O, Campbell CA, *et al.* (2013) The zebrafish granulocyte colony-stimulating factors (Gcsfs): 2 paralogous cytokines and their roles in hematopoietic development and maintenance. *Blood*. 122:3918–28.
12. Barros-Becker F, Romero J, Pulgar A, Feijoo CG. (2012) Persistent oxytetracycline exposure induces an inflammatory process that improves regenerative capacity in zebrafish larvae. *PLoS One.* 7:1–9.
13. van der Vaart M, van Soest JJ, Spaink HP, Meijer AH. (2013) Functional analysis of a zebrafish myd88 mutant identifies key transcriptional components of the innate immune system. *Dis. Models Mech.* 6:841–54.
14. Sepulcre MP, Alcaraz-Pérez F, López-Muñoz A, *et al.* (2009) Evolution of lipopolysaccharide (LPS) recognition and signaling: fish TLR4 does not recognize LPS and negatively regulates NF-kappaB activation. *J. Immunol.* 182:1836–45.
15. Sullivan C, *et al.* (2009) The gene history of zebrafish tlr4a and tlr4b is predictive of their divergent functions. *J. Immunol.* 183:5896–5908.
16. Philip AM, Vijayan MM. (2015) Stress-immune-growth interactions: cortisol modulates suppressors of cytokine signaling and JAK/STAT pathway in rainbow trout Liver. *PLoS One*. 10:e0129299.
17. Remick DG. (2007) Pathophysiology of sepsis. *Am. J. Pathol.* 170:1435–44.
18. Lee WL, Slutsky AS. (2010) Clinical implications of basic research: sepsis and endothelial permeability. *N. Engl. J. Med.* 363:689–91.
19. Avdesh A, *et al.* (2012) Regular care and maintenance of a zebrafish (Danio rerio) laboratory: an introduction. *J. Vis. Exp.* 69:e4196.
20. Nüsslein-Volhard C, Dahm R. (2002) *Zebrafish: Practical Approaches*. New York: Oxford University Press.
21. Kimmel CB, Ballard WW, Kimmel SR, Ullmann B, Schilling TF. (1995) Stages of embryonic development of the zebrafish. *Dev. Dynam*. 203:253–310.
22. Warren HS. (2009) Editorial: Mouse models to study sepsis syndrome in humans. *J. Leukoc. Biol*. 86:199–201.
23. Rieger S, Kulkarni RP, Darcy D, Fraser SE, Köster RW. (2005) Quantum dots are powerful multipurpose vital labeling agents in zebrafish embryos. *Dev. Dyn.* 234:670–81.
24. Li L, Yan B, Shi YQ, Zhang WQ, Wen ZL. (2012) Live imaging reveals differing roles of macrophages and neutrophils during zebrafish tail fin regeneration. *J. Biol. Chem.* 287:25353–60.
25. Gentile LF, Moldawer LL. (2014) HMGB1 as a therapeutic target for sepsis: it's all in the timing! *Expert Opin. Ther. Targets*. 18:243–45.
26. Encinas P, et al. (2013) Identification of multipath genes differentially expressed in pathway-targeted microarrays in zebrafish infected and surviving spring viremia carp virus (SVCV) suggest preventive drug candidates. *PLoS One*. 8:1–19.
27. Wallez Y, Huber P. (2008) Endothelial adherens and tight junctions in vascular homeostasis, inflammation and angiogenesis. *Biochim. Biophys. Acta*. 1778:794–809.
28. González-Mariscal L, Betanzos A, Avila-Flores A. (2000) MAGUK proteins: structure and role in the tight junction. *Semin. Cell Dev. Biol.* 11:315–24.
29. Li Y, Wu Y, Wang Z, Zhang XH, Wu WK. (2010) Fasudil attenuates lipopolysaccharide-induced acute lung injury in mice through the Rho/Rho kinase pathway. *Med. Sci. Monit*. 16:112–18.
30. Yang LL, et al. (2014) Endotoxin molecule lipopolysaccharide-induced zebrafish inflammation model: a novel screening method for anti-inflammatory drugs. *Molecules*. 19:2390–2409.
31. Alexandraki I, Palacio C. (2010) Gram-negative versus gram-positive bacteremia: what is more alarming? *Crit. Care*. 14:161.
32. Barber AE, Fleming BA, Mulvey MA. (2016) Similarly lethal strains of extraintestinal pathogenic Escherichia coli trigger markedly diverse host responses in a zebrafish model of sepsis. *Msphere*. 1:1–19.
33. Goldenberg NM, Steinberg BE, Slutsky AS, Lee WL. (2011) Broken barriers: a new take on sepsis pathogenesis. *Sci. Trans. Med*. 3:88ps25.
34. Morita K, Sasaki H, Furuse M, Tsukita S. (1999) Endothelial claudin: claudin-5/TMVCF constitutes tight junction strands in endothelial cells. *J. Cell Biol.* 147:185–94.
35. Xie J, Farage E, Sugimoto M, Anand-Apte B. (2010) A novel transgenic zebrafish model for blood-brain and blood-retinal barrier development. *BMC Dev. Biol*. 10:76.
36. Yang CH, et al. (2014) Simvastatin attenuates sepsis-induced blood-brain barrier integrity loss. *J. Surg. Res.* 194:591–98.
37. Li Q, Zhang Q, Wang C, Liu X, Li N, Li J. (2009) Disruption of tight junctions during polymicrobial sepsis. *J. Pathol.* 218:210–22.
38. Eadon MT, et al. (2012) Endotoxemia alters tight junction gene and protein expression in the kidney. *Am. J. Physiol. Renal Physiol.* 303: F821–30.
39. Dejana E, Orsenigo F, Lampugnani MG. (2008) The role of adherens junctions and VE-cadherin in the control of vascular permeability. *J. Cell Sci*. 121:2115–22.
40. Philip AM, Jørgensen EH, Maule AG, Vijayan MM. (2014) Tissue-specific molecular immune response to lipopolysaccharide challenge in emaciated anadromous Arctic charr. *Dev. Comp. Immunol.* 45:133–40.
41. Herwald H, Egesten A, eds. (2011) *Sepsis – Pro-Inflammatory and Anti-Inflammatory Responses: Good, Bad or Ugly?* Basel, Switzerland: Karger.
42. Stockhammer OW, Zakrzewska A, Hegedûs Z, Spaink HP, Meijer AH. (2009) Transcriptome profiling and functional analyses of the zebrafish embryonic innate immune response to Salmonella infection. *J. Immunol.* 182:5641–53.
43. Zou J, Secombes C. (2016) The function of fish cytokines. *Biology (Basel)*. 5:23–58.
44. Stein C, Caccamo M, Laird G, Leptin M. (2007) Conservation and divergence of gene families encoding components of innate immune response systems in zebrafish. *Genome Biol.* 8: R251.
45. Okusawa S, Gelfand JA, Ikejima T, Connolly RJ, Dinarello CA. (1988) Interleukin 1 induces a shock-like state in rabbits. Synergism with tumor necrosis factor and the effect of cyclooxygenase inhibition. *J. Clin. Invest*. 81:1162– 72.
46. Schulte W, Bernhagen J, Bucala R. (2013) Cytokines in sepsis: Potent immunoregulators and potential therapeutic targets. An updated view. *Mediators Inflamm.* 6:165974-90
47. Cinel I, Opal SM. (2009) Molecular biology of inflammation and sepsis: a primer. *Crit. Care Med.* 37:291–304.
48. Hinshaw LB. (1996) Sepsis/septic shock: participation of the microcirculation: an abbreviated review. *Crit. Care Med.* 24:1072–78.
49. Secor D, et al. (2010) Impaired microvascular perfusion in sepsis requires activated coagulation and P-selectin-mediated platelet adhesion in capillaries. *Intensive Care Med.* 36:1928–34.
50. Hotchkiss RS, Monneret G, Payen D. (2013) Immunosuppression in sepsis: a novel understanding of the disorder and a new therapeutic approach. *Lancet Infect. Dis*. 13:260–68.
51. Makino I, Tajima H, Kitagawa H, *et al.* (2015) A case of severe sepsis presenting marked decrease of neutrophils and interesting findings on dynamic CT. *Am. J. Case Rep*. 16:322–327.
52. Gregoire M, Tadie J-M, Uhel F, Gacouin A, *et al.* (2016) HMGB1 induces neutrophil dysfunction in experimental sepsis and in patients who survive septic shock. *J. Leukoc. Biol*. 101:1281-7
53. Eisa-Beygi S, Wen XY. (2015) Could pharmacological curtailment of the RhoA/Rho-kinase pathway reverse the endothelial barrier dysfunction associated with Ebola virus infection? *Antiviral Res.* 114:53–56.
54. Winata CL, et al. (2009) Development of zebrafish swimbladder: The requirement of hedgehog signaling in specification and organization of the three tissue layers. *Dev. Biol.* 331:222–36.
55. Hall FG. (1924) The functions of the swim bladder of fishes. *Biol. Bull.* 47:79-126
56. Pelster B. (1995) Metabolism of the swimbladder tissue. In: *Biochemistry and Molecular Biology of Fishes.* Elsevier, Amsterdam, pp. 101–18.

Cite this article as: Philip AM, *et al.* (2017) Development of a zebrafish sepsis model for high-throughput drug discovery. *Mol. Med.* 23:134–48.